

Article

Lithofacies Characteristics and Pore Controlling Factors of New Type of Permian Unconventional Reservoir in Sichuan Basin

Rong Li ^{1,2,*}, Zhifu Xiong ^{3,*}, Zecheng Wang ^{1,2}, Wuren Xie ^{1,2}, Wenzheng Li ¹ and Jiuzhen Hu ^{4,*}

¹ Research Institute of Petroleum Exploration & Development, PetroChina, Beijing 100083, China
² CNPC Key Laboratory of Natural Gas Accumulation and Development, Langfang 065007, China
³ Sinopec Exploration Company, Chengdu 610041, China
⁴ School of Geosciences, Yangtze University, Wuhan 430100, China
* Correspondence: li_rong@petrochina.com.cn (R.L.); xiongzf.ktnf@sinopec.com (Z.X.); hujiuzhen@163.com (J.H.)

Abstract: Alongside volcanic eruptions in the middle and late Permian, the sedimentary environment and process changed, and the lithofacies characteristics varied conspicuously in the marine deposits of the Sichuan Basin (China). The tuffaceous rocks, as a new type of unconventional reservoir, provide strong evidence for marine and volcanic influences on the lithology and reservoir potential of the rocks. With experimental studies relying on field outcrops, thin sections, scanning electron microscopy and whole-rock X-ray diffraction (XRD), the researchers analyzed the lithofacies characteristics, pore types and controlling factors on the various types of pores in the tuffaceous rocks. We identified three lithofacies types in this new type of Permian reservoir in the Sichuan Basin, namely tuff, sedimentary tuff, and tuffaceous mudstone. The mineral composition of the three lithofacies includes quartz, feldspar, carbonate minerals, pyrite, and clay, among which feldspar is mainly potassium feldspar. Tuff has high tuff content, and the lowest clay and TOC content; tuffaceous mudstones have the highest clay and TOC content, and the lowest tuff content. The pore types of the tuffaceous rocks are mainly nano-scale shrinkage pores, with a small number of intergranular pores including intragranular pores, intergranular pores, and organic pores. The shrinkage pores account for 81.9% of the total pores, and organic pores account for 11.2% of the total pores. In the tuffaceous rocks, the tuff content, quartz and feldspar content, and pyrite content are inversely correlated with porosity, while the clay content and TOC content are positively correlated with porosity. The porosity of tuff is the lowest, followed by sedimentary tuff, and the porosity of tuffaceous mudstone is the highest. Tuffaceous rocks form many micropores in the process of devitrification. Organic matter pyrolysis and organic acid dissolution also increase the reservoir space and porosity of the reservoir. This new type of reservoir has the ability of hydrocarbon accumulation along with the reservoir performance, and thus it has greater exploration prospects.

Keywords: unconventional reservoir; tuff; sedimentary tuff; tuffaceous mudstone; lithofacies; porosity



Citation: Li, R.; Xiong, Z.; Wang, Z.; Xie, W.; Li, W.; Hu, J. Lithofacies Characteristics and Pore Controlling Factors of New Type of Permian Unconventional Reservoir in Sichuan Basin. *Processes* **2023**, *11*, 625. <https://doi.org/10.3390/pr11020625>

Academic Editor: Yidong Cai

Received: 6 January 2023

Revised: 13 February 2023

Accepted: 16 February 2023

Published: 18 February 2023



Copyright: © 2023 by the authors. Licensee MDPI, Basel, Switzerland. This article is an open access article distributed under the terms and conditions of the Creative Commons Attribution (CC BY) license (<https://creativecommons.org/licenses/by/4.0/>).

1. Introduction

In recent years, pyroclastic reservoirs have been discovered globally, including some sedimentary basins in Japan, Cuba, the United States, New Zealand and Turkey, as well as in the Ordos, Junggar, Jiuquan, Bohai Bay, Erlian and Songliao Basins in China [1–8]. In particular, the successful oil testing of Permian tuff in the Santanghu Basin in 2013 confirmed the importance of tuff reservoirs, leading to interest in this new type of tuff reservoir.

During the Late Permian of the Late Paleozoic, the marine sedimentary environment and depositional processes changed, and a volcanic eruption occurred in the southwest of China, forming the Emeishan Large Igneous Province (ELIP) [9–19]. It consists of a large amount of basaltic rocks, pyroclastic lavas, and tuffaceous rock [20–22]. Among them, the test of the Permian basalt of the ZGI well obtained a daily gas production of 256,100 mcf

The lithology of the pyroclastic rocks is dominated by pyroclastic lavas such as brecciated lavas, tuff brecciated lavas and tuff-bearing brecciated lavas. These rocks are mainly found in the Chengdu-Jianyang area, with a thickness of 200 to 350 m, thinning to less than 50 m towards the margin. The tuffaceous rocks are the transition from the volcanic to the sedimentary facies and are formed by the redeposition of volcanic debris after being transported by seawater. The marine tuffaceous rocks are generally sediment-stratified and structured, with a wide distribution, but a relatively thin thickness of 10 to 20 m in the Sichuan Basin [39–41] (Figure 1B).

3. Samples and Methods

We selected 26 samples from typical wells with an average sampling spacing of less than 1 m for testing and analysis. The identification of the samples in plain and cast thin sections was performed in the Sedimentary Geology Laboratory of Chengdu University of Technology. Scanning electron microscopy and energy spectroscopy analyses and rock physical properties testing were completed at the Key Laboratory of Oil and Gas Reservoir Exploration and Development, Chengdu University of Technology. Total organic carbon (TOC) and X-ray diffractometer (XRD) analyses were completed at the Experimental Research Centre of Wuxi Institute of Petroleum Geology, Sinopec Petroleum Exploration and Development Research Institute. All samples were crushed and ground to below 200 mesh. For the TOC analysis, approximately 200 g of samples were firstly decarbonated with 10% dilute hydrochloric acid at 60 degrees; we then rinsed the samples to remove the remaining HCl. The samples were finally dried with a carbon and sulfur analyzer. Based on the relevant Chinese National Test Standards, the analytical results have an error of 0.5%. Whole rock mineral analysis was carried out using a Bruker D8 X-ray diffractometer. We loaded powdered samples and scanned them with the diffractometer, obtaining whole rock data from 5 to 90 degree scans.

4. Results

4.1. Observation of Outcrop and Core Samples

A typical tuffaceous succession is exposed in the standard section of the Permian Wujiaping Formation at Daping Village, Wangcang County, Guangyuan City. The tuffaceous rocks are underlain by a thin-medium thick, grey-black mudstone interbedded with thin carbonaceous mudstone, and overlain by a thick layer of dark grey argillaceous (Figure 2A). The tuffaceous rocks can be divided into four sub-layers. The first sub-layer is a 54 cm thick, light grey fused breccia, containing a small amount of breccia, which is characterized by hydrothermal dissolution during the burial period, with the conglomerate partially dissolved and solution holes formed, associated with pyrite in the upper part (Figure 2B). The second sub-layer is a mixed colored breccia with a breccia content between 40% and 50%, where hydrothermal alteration is particularly evident, with some of the breccia being dissolved, forming more solution holes filled with pyrite (Figure 2C). The third sub-layer is a breccia-bearing tuff, where the breccias have been dissolved, forming intra-gravel cavities and pyrite fillings (Figure 2D). The fourth sub-layer is a black carbonaceous tuff with distinct lamination (Figure 2E).

Under the microscope, the tuffaceous rocks are mostly composed of pyroclastic fragments, argillaceous, and carbonate minerals, which are unevenly distributed. Among them, the pyroclastic fragments are mainly vitric fragments, quartz, feldspar crystal fragments and lithic fragments; feldspar is mostly argillized; vitric fragments and lithic fragments are mostly devitrified into clay, and part of which are replaced by powdery dolomite; carbonate minerals such as dolomite and calcite represent minor components, generally less than 6%, and play a cementing role between the pyroclastic fragments; and the dolomite autocrysts are fewer. The size of the pyroclastic fragments is highly variable, concentrated in the range from 0.1 mm to 0.5 mm, and the distribution of the pyroclastic fragments is uneven, with different morphologies, such as sickle-shaped, crescent-shaped, and bow-shaped. The lithic fragments, with a particle size of generally over 0.050 mm and up to 0.500 mm at most,

are mainly in round shapes and partly in irregular shapes and composed of rhyolite, tuff lithic fragments and hyaloclastite. The crystal fragments are dominated by quartz crystal fragments, with a small quantity of feldspar and mica crystal fragments. They are often in angular and fragmented shapes, with a particle size from 0.100 mm to 0.050 mm. The vitric fragments have a particle size from 0.100 mm to 0.050 mm, and are rarely in rigid fractures (Figure 3).

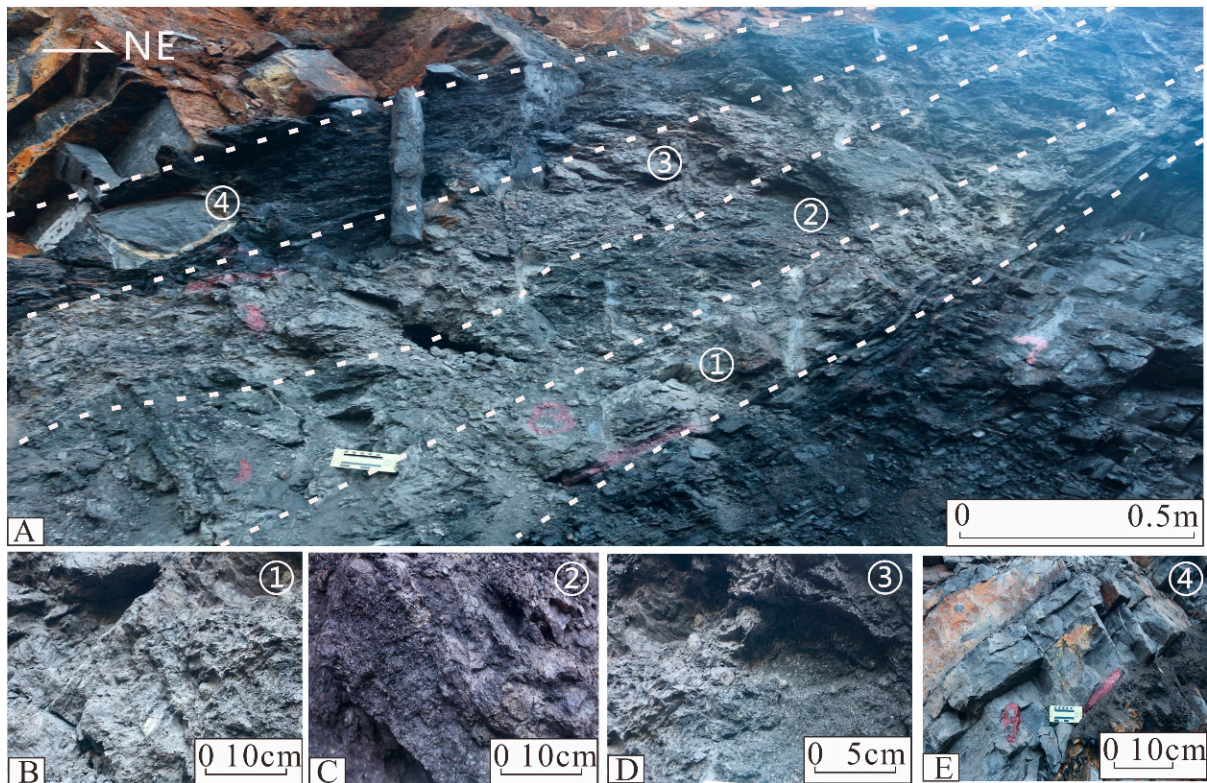


Figure 2. Typical lithological characteristics of the Longtan Formation. ((A) Full view of the Daping Village section, showing a tuffaceous succession overlies grey-black thin- to medium-bedded mudstone interbedded with thin carbonaceous mudstone and underlies dark grey argillaceous layer; (B) light grey fused breccia; (C) motley breccia; (D) breccia-bearing tuff; and (E) black carbonaceous sedimentary tuff).

The outcrop and core observations reveal that the tuffaceous rocks are usually tight, and the dissolution pores visible to naked eye are largely undeveloped, with a few laminated fractures visible. Thin section and scanning electron microscope (SEM) observations show that the tuffaceous rocks are rich in pore types, which can be divided into primary and secondary pores. Primary pores include shrinkage pores (Figure 4A,B), intergranular pores (Figure 4C), etc. Secondary pores consist of dissolution pores (Figure 4C), secondary intergranular pores (Figure 4D), organic pores (Figure 4E), etc. These also have some microcracks (Figure 4F). Due to the unstable vitroclastic composition in the pyroclastic fragments, the destabilization results in volume reduction and the formation of shrinkage pores. In addition, during the alteration process or the transformation of unstable materials at a later stage, dissolution can occur when acidic fluids are encountered, resulting in the formation of secondary dissolution micropores.

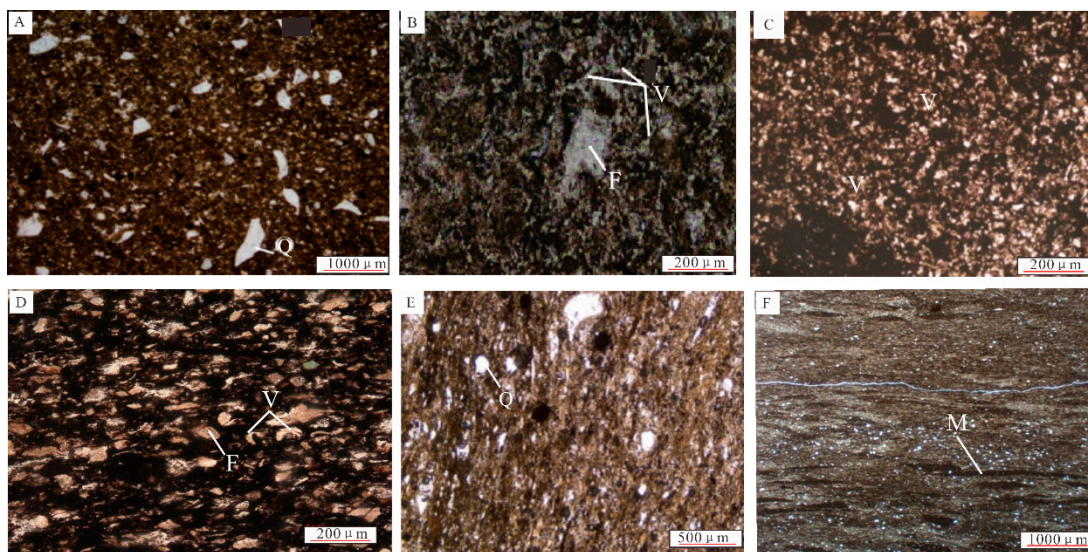


Figure 3. Thin sections of the Longtan Formation/Wujiaping Formation showing typical lithological features. ((A) Fushi 1 well, Wu 2 Member, 4832 m, crystalline tuff, PPL; (B) Yuan 7 well, Wu 2 Member, 6915 m, crystalline tuff, PPL; (C) Longgang 2 well, Wujiaping Formation, 5972.08 m, sedimentary tuff with tuffaceous texture, PPL; (D) Nanchong 2 well, Longtan Formation, 5869 m, sedimentary tuff with tuffaceous texture, PPL; (E) Ping Shang section, Longtan Formation, tuffaceous mudstone, PPL; and (F) Huaying Shan section, bottom of Longtan Formation, tuffaceous mudstone, PPL. F—Feldspar; M—Mud; Q—Quartz; V—Vitric; PPL—plane polarized light).

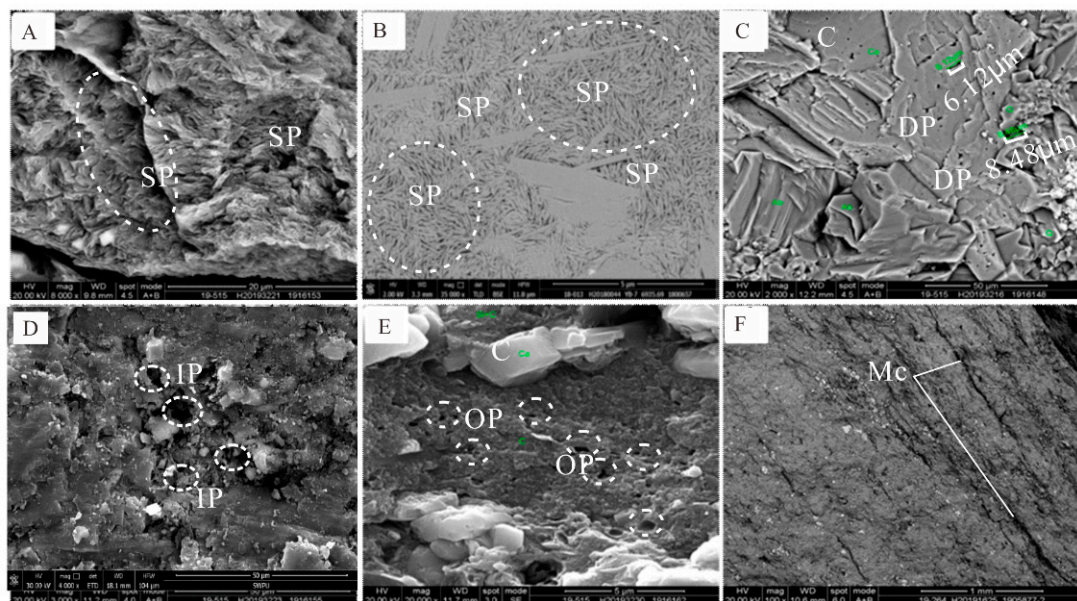


Figure 4. SEM features of typical reservoir space in tuffaceous succession. ((A) Tuff, contraction holes developed between mica and clay flakes, 6811.9 m, well SY1-1. (B) Tuffaceous mudstone with contraction holes in clay minerals, 6935.69 m, well Y7. (C) Sedimentary tuff, calcite solution holes enlarged, about 6 mm or less, intergranular pores colloidal quartz and sodium feldspar, 4945.65 m, well M1. (D) Sedimentary tuff with development of intergranular solution holes, 5972.08 m, well L2. (E) Sedimentary tuff with development of organic matter holes, 6867.21 m, well SY1-1; f. 5972.08 m, well L2. (F) Tuffaceous mudstone with fracture development, 6936.07 m, well Y7. C—Calcite. DP—Dissolved pores; IP—Intercrystal pores; Mc—Microcrack; OP—Organic pores, SP—Shrinkage pores).

4.2. Quantitative Analysis of Mineral Components

The X-ray diffraction results of the whole-rock minerals from all samples show that the minerals of tuffaceous rocks are mainly composed of clay, quartz, plagioclase, potassium feldspar, calcite, dolomite, ankerite, and pyrite (Figure 5). Among them, quartz minerals content ranged from 3.8% to 29.3%, with an average of 14.2%. The quartz minerals content in the typical well section has regular variation characteristics, with an overall gradual increase upwards. The clay minerals are mainly illite/smectite formations and illite, with an overall less than 74.9% and an average of 42.6%. There are no samples without clay minerals, and their content varies in the opposite direction to quartz, with a gradual upward decrease in content. The feldspar minerals include potassium feldspar and plagioclase, with their contents ranging from 0 to 23.2%, averaging 9.9%; the plagioclase content is more stable and the potassium feldspar content is lesser, not exceeding 1%. Carbonate minerals mainly comprise calcite and dolomite, with locally high levels of ankerite, whose total content ranges from 8.48% to 52.54%, with an average value of 28.1% and a gradual upward decrease in carbonatite minerals. Pyrite is detected in almost all core samples, of which the content ranges from 0 to 9.9%, with an average of 5.2%.

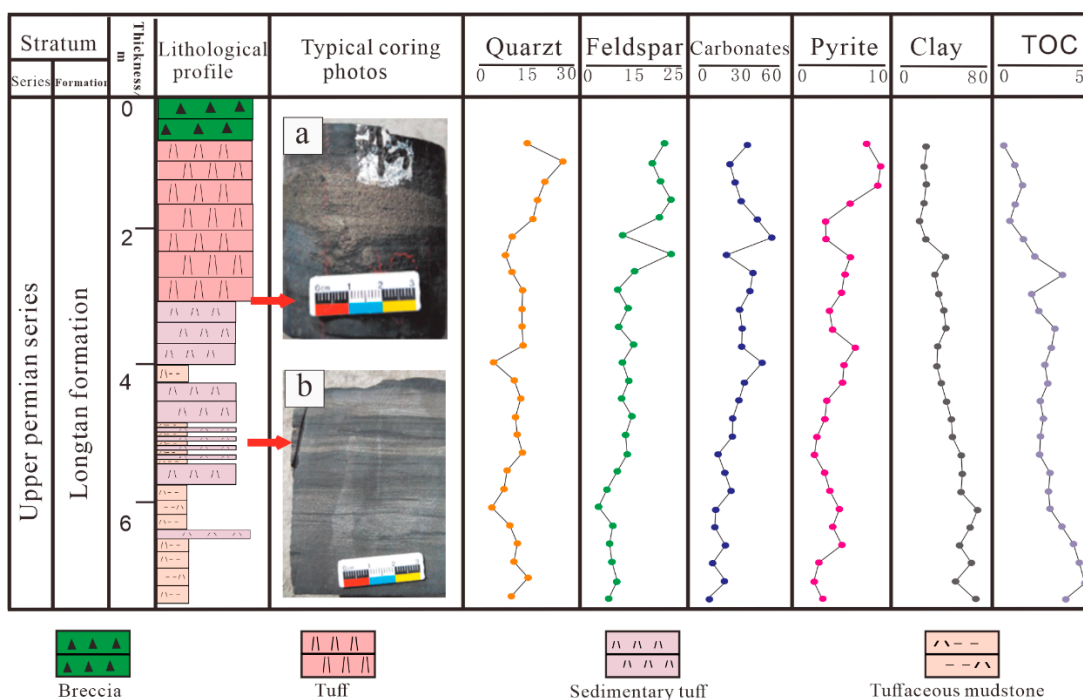


Figure 5. Main mineral components of tuff succession of a typical well.

4.3. Organic Matter Abundance

An organic carbon test indicates that the organic carbon in the tuffaceous rocks ranged from 0.30% to 4.66%, with an average of 2.48%. Most samples have a TOC ranging from 1% to 4% (Figure 5). The low values of organic carbon are all found at the bottom of the tuff succession and the high values are all found in the upper part of the tuffaceous rocks, showing increasing trends from the top toward the bottom. The organic carbon content of the Permian Wujiaping Formation mudstones in the Sichuan Basin ranges from 1.21% to 4.23%, with an average value of 2.65%; the extraction of chloroform bitumen “A” ranges from 0.11% to 0.48%, with an average value of 0.18%; the hydrocarbon potential ranges from 2.52 to 60.43 mg/g, with an average value of 25.48 mg/g. The organic carbon of the selected tuffaceous mudstone ranges from 2.5% to 4.66%, with an average of 3.48%; the extraction of chloroform bitumen “A” ranges from 0.08% to 2.25%, with an average value of 0.87%; and the hydrocarbon potential varies widely, ranging from 8.9 mg/g to 140.35 mg/g, with an average of 45.97 mg/g (Figure 6).

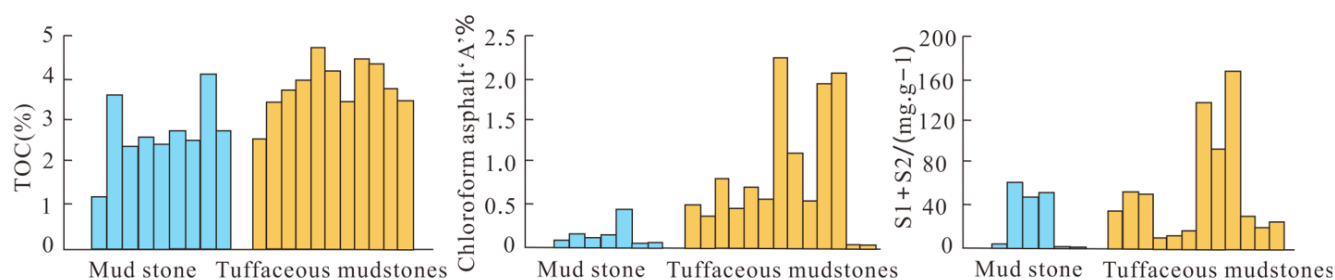


Figure 6. Comparison of organic matter abundance between mudstones and tuffaceous mudstones of the Wujiaping Formation in the Sichuan Basin.

4.4. Lithofacies

Pyroclastic rock with volcanic sedimentary facies developed in the research area belongs to the tuffaceous rocks. They can be classified as normal pyroclastic rocks, sedimentary pyroclastic rocks, and pyroclastic sedimentary rocks according to their volcanic material content and diagenesis [42–44] (Table 1). The normal pyroclastic rocks in the area are dominated by tuffs, the sedimentary pyroclastic rocks are dominated by sedimentary tuffs, and the pyroclastic sedimentary rocks are dominated by tuffaceous mudstones, with the latter two types of rocks having distinct lamination. A small number of bioclasts, including spicule and foraminifer, can be seen locally, and silicification was spotted inside some of the bioclasts. The tuffaceous rocks are characterized by high gamma, high sonic differential time, and low resistance, which are distinctly different from the other rock types. The natural gamma values range from 65 API to 145 API, compensated neutron values range between 10 and 45 P·U, sonic differential time values range from 62 $\mu\text{s}/\text{ft}$ to 107 $\mu\text{s}/\text{ft}$, and resistivity values range from 5 $\Omega\cdot\text{m}$ to 20 $\Omega\cdot\text{m}$. The tuffs have natural gamma values of 14–45 API, compensated neutron values between 0 P·U and 4 P·U, sonic differential time values between 44 $\mu\text{s}/\text{ft}$ and 61 $\mu\text{s}/\text{ft}$ and resistivity values between 50 $\Omega\cdot\text{m}$ and 10,000 $\Omega\cdot\text{m}$; argillaceous limestones have natural gamma values of 35–280 API, compensated neutron values between 2 P·U and 12 P·U, sonic differential time values between 50 $\mu\text{s}/\text{ft}$ and 67 $\mu\text{s}/\text{ft}$ and resistivity values between 90 $\Omega\cdot\text{m}$ and 1000 $\Omega\cdot\text{m}$ (Figure 7).

Table 1. Classification of Permian tuff successions in the Sichuan Basin.

Types	Rocks	Component	Sedimentary Structures
Normal pyroclastic rocks	Tuff	Composition of pyroclastic debris ranges between 75% and 90%	Insignificant stratification
Sedimentary pyroclastic rocks	Sedimentary tuff	Composition of pyroclastic debris ranges between 50% and 75%; Composition of terrestrial debris <50%	Significant stratification
Pyroclastic sedimentary rocks	Tuffaceous mudstone	Composition of clay mineral >50%; Composition of pyroclastic debris >10%	Significant stratification

4.4.1. Tuff

The tuff is predominantly in grey, with 75% to 90% pyroclastic content and a fine to medium grain texture; the grain size ranges approximately between 0.05 mm and 0.5 mm; and natural gamma-ray (GR) values range from 65 to 110 API, with an average value of 85 API. Based on the results of a large number of thin sections, the tuff contains approximately 75% to 90% pyroclastic, quartz and feldspar. The margins of rock debris are irregular and complex in shape; including angular, sickle, bowed and crescent shape; and chaotically arranged. The external appearance of the rocks is loose, rough, porous, and mostly massive in structure. The

feldspar and quartz content of tuff varies from 18.7% to 43.76%, the clay content is between 18.51 to 24.42% and there is an average TOC content of 1%.

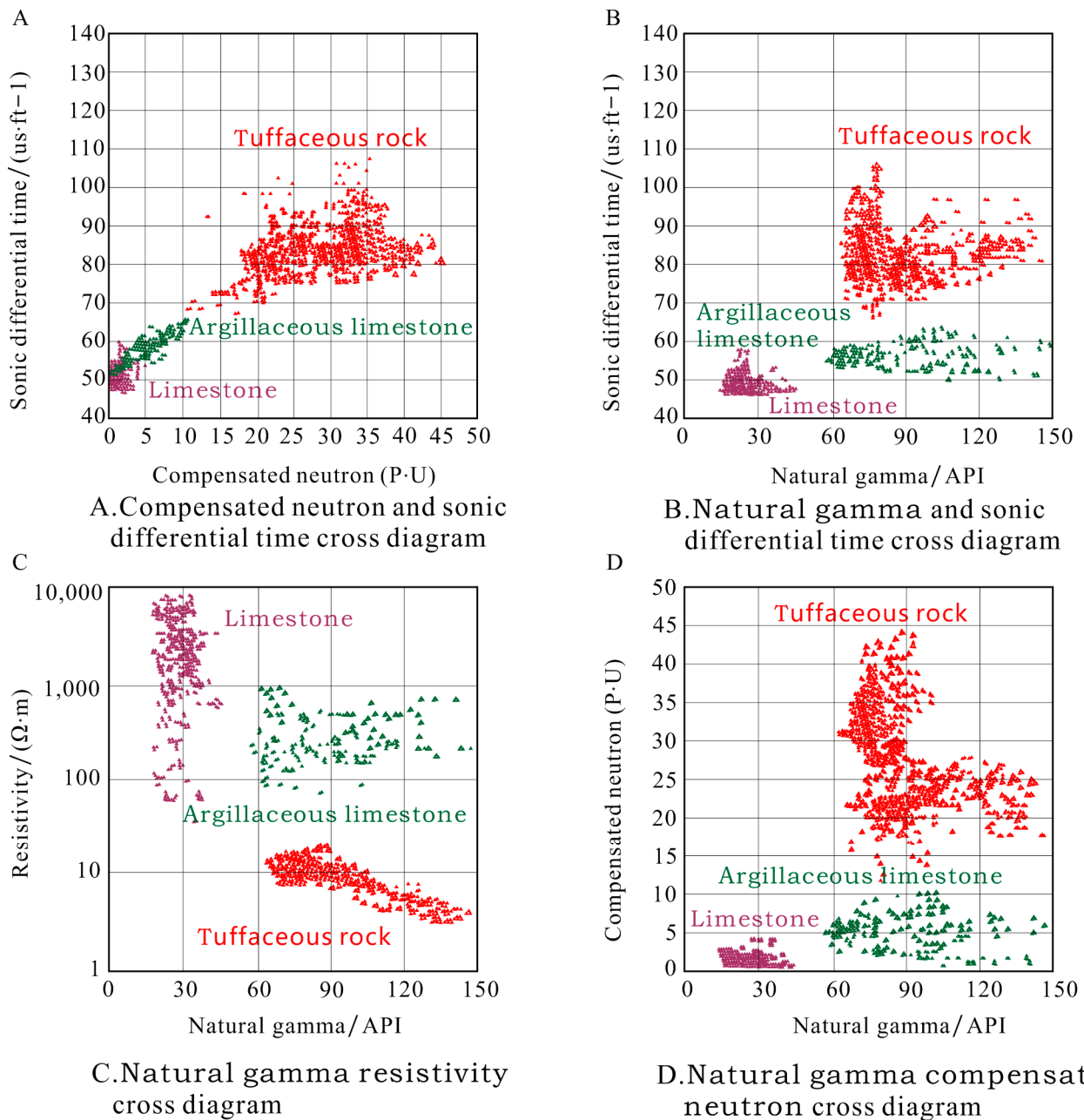


Figure 7. Lithology identification diagrams of the Wujiaping Formation.

4.4.2. Sedimentary Tuff

Sedimentary tuff is mainly dark grey, with 50% to 75% pyroclastic content, which is characterized by a fine-grained structure with a grain size of less than 0.1 mm. The natural gamma-ray (GR) values range from 69 API to 120 API, with an average value of 93 API. Based on the results of the analysis of thin sections, the sedimentary tuff contains 50% to 60% pyroclastic, quartz and feldspar, and 30% to 40% clay. Most of the clay minerals are derived from volcanic debris alteration. The sedimentary tuffs are clearly stratified. The feldspar content of the sedimentary tuff ranges from 12.72% to 29.25%; the clay content ranges from 24.42% to 49.44%, and the average TOC content is 2.4%.

4.4.3. Tuffaceous Mudstone

The tuffaceous mudstone, mostly grayish black, is composed of pyroclastic material and sedimentary clast, with a relatively low pyroclastic content of less than 50%. The pyroclastic material is more angular than the sedimentary clast, and is poorly sorted and rounded. The natural gamma-ray (GR) values range from 92 API to 145 API, with an average value of 109 API. According to the results of a large number of thin sections, the tuffs contain less than 50% volcanic clasts, quartz and feldspar, and more than 50% clay, with an average TOC content of 3.5%.

From the analysis of the outcrop and core data, it is evident that the sedimentary tuff and tuffaceous mudstone are often horizontally laminated, with thicknesses varying from millimeters in the thinnest layers to 10 cm in the thickest layers. The cores are locally enriched in pyrite, mostly porphyritic and locally laminated. The pyrite varies in size from 1 mm to 5 cm, unevenly distributed.

5. Discussion

5.1. Pore Types

Shrinkage pores: the main pores in the tuffaceous rocks have two types of genesis, one is the transformation of volcanic detrital material to stable minerals such as quartz and feldspar during the devitrification process, resulting in volume reduction and thus forming shrinkage pores; the other type is the formation of clay minerals during the accountable alteration process of volcanic detrital material, while clay minerals have a shrunk diagenetic volume to form shrinkage pores. Although widely distributed in tuff, sedimentary tuff, and tuffaceous mudstone, shrinkage pores are most common in tuffaceous mudstone.

Dissolved pores: it mainly includes inter-granular and intra-granular dissolved pores. The unstable mineral components in feldspar and carbonate minerals are susceptible to dissolution during the process of replacement alteration of pyroclastic material, forming inter-feldspar dissolution pores and dissolution pores in carbonate minerals.

Intercrystal pores: during the process of devitrification, the formation of quartz and feldspar and the rearrangement of mineral crystals form intercrystal pores. The process of replacement alteration to form various types of secondary minerals and carbonate minerals can also form intercrystal pores.

Organic pores: during the process of replacement alteration and devitrification, organic matter is dissolved by organic acids, forming organic pores, which are usually small, with a pore size of several hundred nanometers.

Fractures: outcrop and core observations display that low-angle interlamellar fractures developed parallel to layers. The millimeter wide fractures are locally filled. More unfilled interlamellar fractures were observed in thin section and SEM, which are more common in tuffaceous mudstones, with fracture widths of nanometer scale.

We selected typical tuffaceous rock samples for a comparative analysis of the reservoir space and found that shrinkage pores were the most abundant in clay, accounting for an average of up to 81.9%, while organic matter pores accounted for 11.2% and intergranular dissolved pores, intragranular dissolved pores and intercrystal pores accounted for 6.9% (Figure 8).

5.2. Mineral Enrichment

5.2.1. Sulphur-Bearing Mineral Enrichment

In conventional logging and core data, the fine-grained sediments in this section are mainly argillaceous limestone, marlstone, and mudstones. From whole-rock X-ray diffraction data, the section contains stable volcanic ash, mostly felsic rocks, and there is a good positive correlation between volcanic ash and pyrite content. The association of volcanic material with pyrite is not only seen in this Permian section of the Sichuan Basin, but also in sulfide iron ores in many parts of the world, and volcanism is an important formation mechanism for this type of ore [45–47]. The chemical formula for pyrite is FeS_2 , and the link between volcanic material and pyrite genesis can be divided into sulfur-

supplying and iron-supplying sources, with the sulfur-supplying source playing a major role. The main source of sulfur is the transport of sulfur components stored in the magma to seawater through volcanic eruptions. In the southwest Sichuan Basin, volcanoes erupt strongly, emitting ash clouds rich in sulfur dioxide gas. During the intervals between eruptions, the craters and nearby volcanic vents are capable of ejecting a continuous stream of sulfur dioxide gas. Volcanic ash is ejected as ash clouds during volcanic eruptions along with strong acidic gases such as sulfur dioxide. Under high temperature conditions, the sulfuric aerosols and sulfur dioxide oxidize to form sulfuric acid, which strongly corrodes the ash surface, resulting in a sulfate containing a surface salt film. Volcanic ash injected into seawater can release large amounts of sulfate ions in a short period of time. In the north and the east of Sichuan, underwater crater eruptions are the prevailing case, where the magma is in more intimate contact with seawater. The dissolved sulfur dioxide in the magma degasses from the magma and then dissolves directly in seawater increasing the sulfate ion content of the water column.

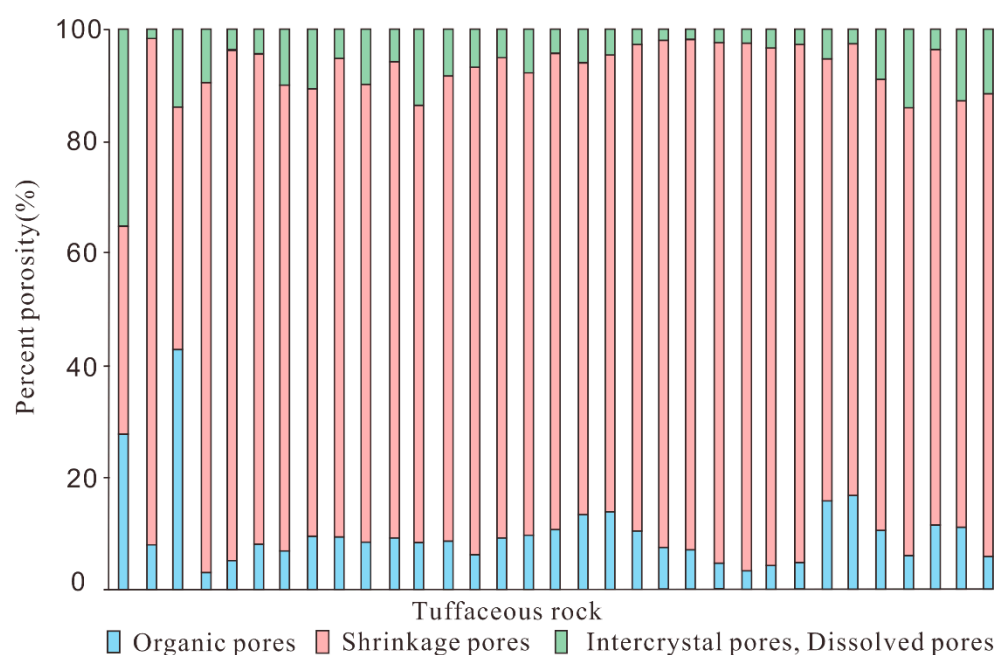


Figure 8. Reservoir space of tuffaceous rock types in the Wujiaping Formation, Sichuan Basin.

5.2.2. Organic Matter Enrichment

In terms of organic matter abundance, both mudstone and the tuffaceous mudstone in the Wujiaping Formation are good hydrocarbon source rocks, but the tuffaceous mudstone is higher than its contemporaries in terms of organic carbon, chloroform asphalt “A” and hydrocarbon generating potential (Figure 8). It shows that volcanic ash has a significant enrichment effect on the organic matter in hydrocarbon source rocks. When elements such as P from the volcanic material enter the sea water to provide rich nutrients, it promotes the proliferation of aquatic organisms and increases paleoproductivity, thus increasing organic matter abundance and forming abundant organic pores.

5.3. Controlling Factors

5.3.1. Relationship between Mineral Composition and Pore

In order to clarify the controlling factors on the porosity of tuff succession, a large number of samples were selected to study the variation of mineral fraction and porosity of each tuff succession. From the scatter plot, we found that the overall porosity of the tuff succession is high, with an effective porosity greater than 2% and an average porosity of 5.24%, ranging from 2.1% to 8.2%. However, the scatter plot shows that porosity is mostly comprised between 3% and 7% (Figure 9). When the quartz content of the tuff

succession is low, the porosity is high; as the quartz content increases, the porosity shows an overall decreasing trend. There is no particularly clear relationship between changes in feldspar content and porosity. In general, there is an inverse correlation between feldspar and quartz content and porosity variation, i.e., as feldspar and quartz content decreases, porosity increases. The variation in pyrite content was also roughly inversely correlated with porosity, i.e., when the pyrite content was low, the porosity was relatively high. However, the change in porosity is less pronounced after the pyrite content is greater than 10%. There is a clear positive correlation between clay content and porosity, with porosity increasing as the clay content increases.

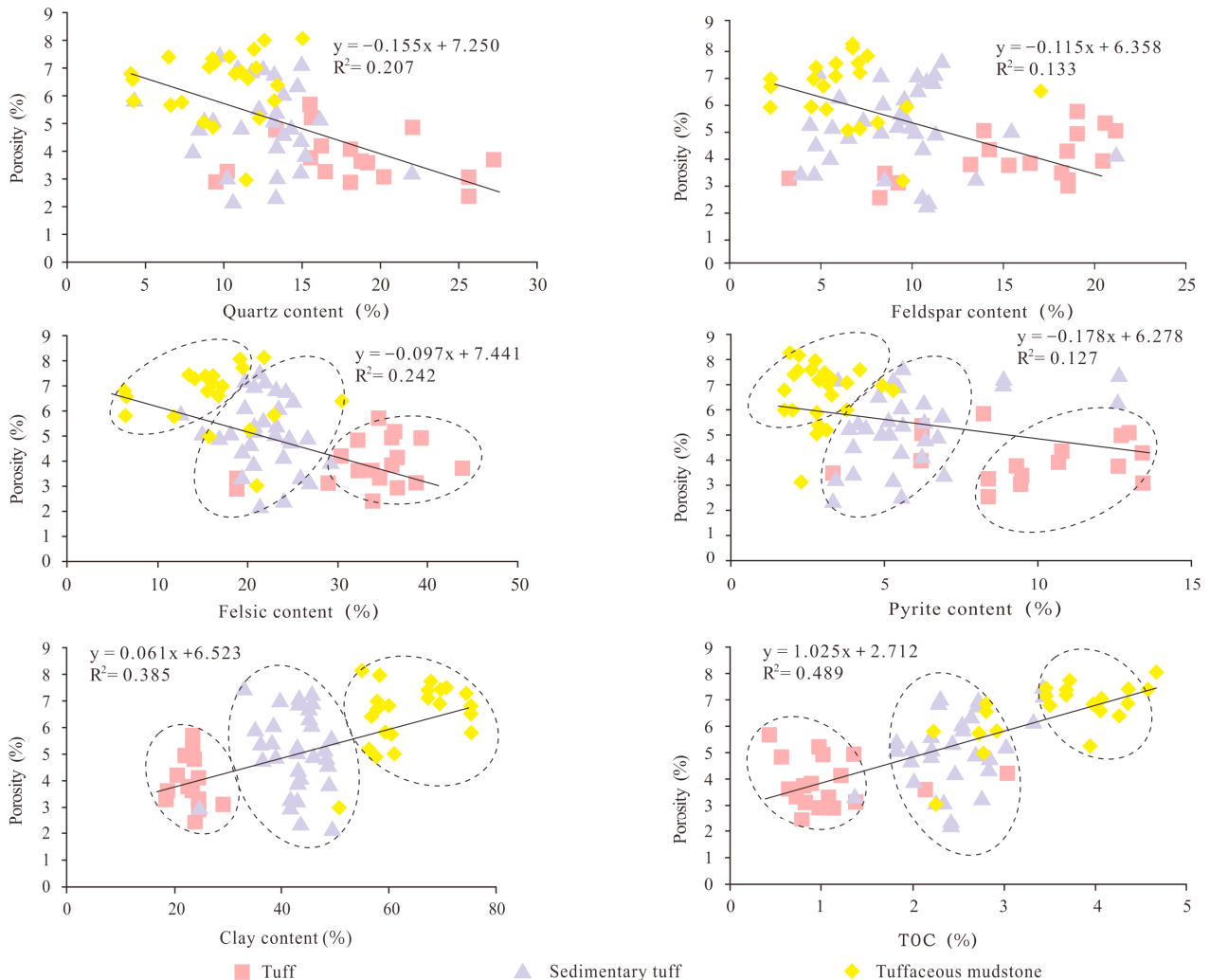


Figure 9. Scatter plot of mineral composition, TOC and porosity.

5.3.2. Relationship between TOC Content and Pore

Shrinkage pores, organic pores and fractures are common in tuffaceous rocks, which have more similarities to shale [48–50]. Whether the organic carbon affects the pore space is an important issue in the study of tuffaceous rocks. Based on a large number of sampling analyses, we found that the porosity of tuffaceous rocks are mostly higher than 2%, and when the organic carbon content is less than 1%, the porosity varies from 2.3% to 5.8%, with an average porosity of 3.9%. However, there is an overall trend of increasing porosity as the organic carbon content increases (Figure 9).

5.3.3. Relationship between Tuffaceous Component and Pore

There are three lithofacies types in the studied tuffaceous rocks, including tuff, sedimentary tuff, and tuffaceous mudstone. The tuff content of the three lithofacies types varies considerably. The tuffs have a relatively high tuff content of 75% to 90%. Sedimentary tuffs have a tuff content of 50% to 75%. The tuffaceous mudstones have a smaller tuff content, between 10% and 50%. The overall porosity of the tuffs is relatively low, mostly ranging from 2.4% to 5.7% and mainly concentrating at 3% to 4%, with an average porosity of 3.86%; the sedimentary tuffs are mainly comprised between 2.2% and 7.5%, with an average porosity of 5.09%; the tuff mudstones have the highest porosity, mainly comprised between 5% and 8%, with an average porosity of 6.5% (Figures 9 and 10). The porosity is strongly influenced by the tuff content. In contrast, clay content variation is significantly influenced by lithology, with the tuffs having the lowest clay content and the lowest average porosity. Tuffs also have the lowest organic carbon content and the lowest porosity; in contrast, tuffaceous mudstones have the highest clay and organic carbon content, with the highest average porosity.

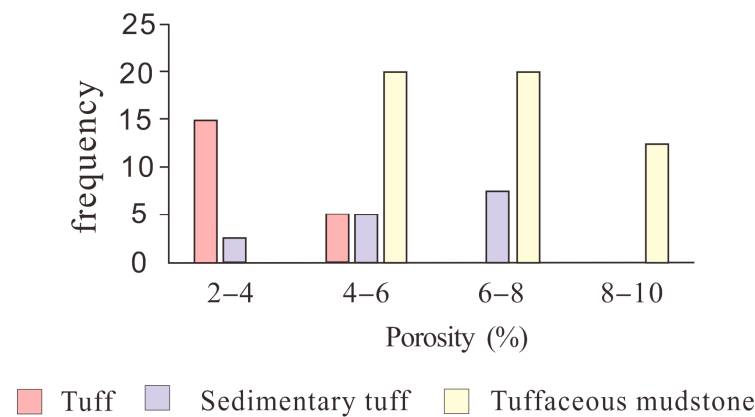


Figure 10. Distribution of porosity in tuffaceous rocks.

In summary, according to the relationship between porosity and the variation of tuff composition in the three lithofacies, we find that the higher content of volcanic material, the lower the porosity will be; the higher the content of clay minerals, the higher the porosity will be. Tuffs have the highest tuff content and the lowest clay content, so they have the lowest porosity; tuffaceous mudstones have the lowest tuff content and the highest clay content, so they have the highest porosity.

5.3.4. Relationship between Devitrification and Dissolution and Porosity

In the storage space of tuffaceous rock samples, the shrinkage pores between clays are the most, accounting for 81.9% on average, the organic matter pores account for 11.2%, and the intergranular dissolved pores, intragranular dissolved pores, and intercrystalline pores account for 6.9%. It can be seen that shrinkage pores and dissolution pores are most important storage spaces, except for organic matter pores (Figure 8). In the process of devitrification, tuffaceous rocks transform into quartz microcrystals (Figure 11). With the formation of clay, due to the smaller volume, a large number of micropores are released. In the process of pyrolysis of organic matter, the organic acid formed dissolves feldspar and carbonate minerals, forming a large number of dissolution pores. These processes all increase the porosity of the reservoir.

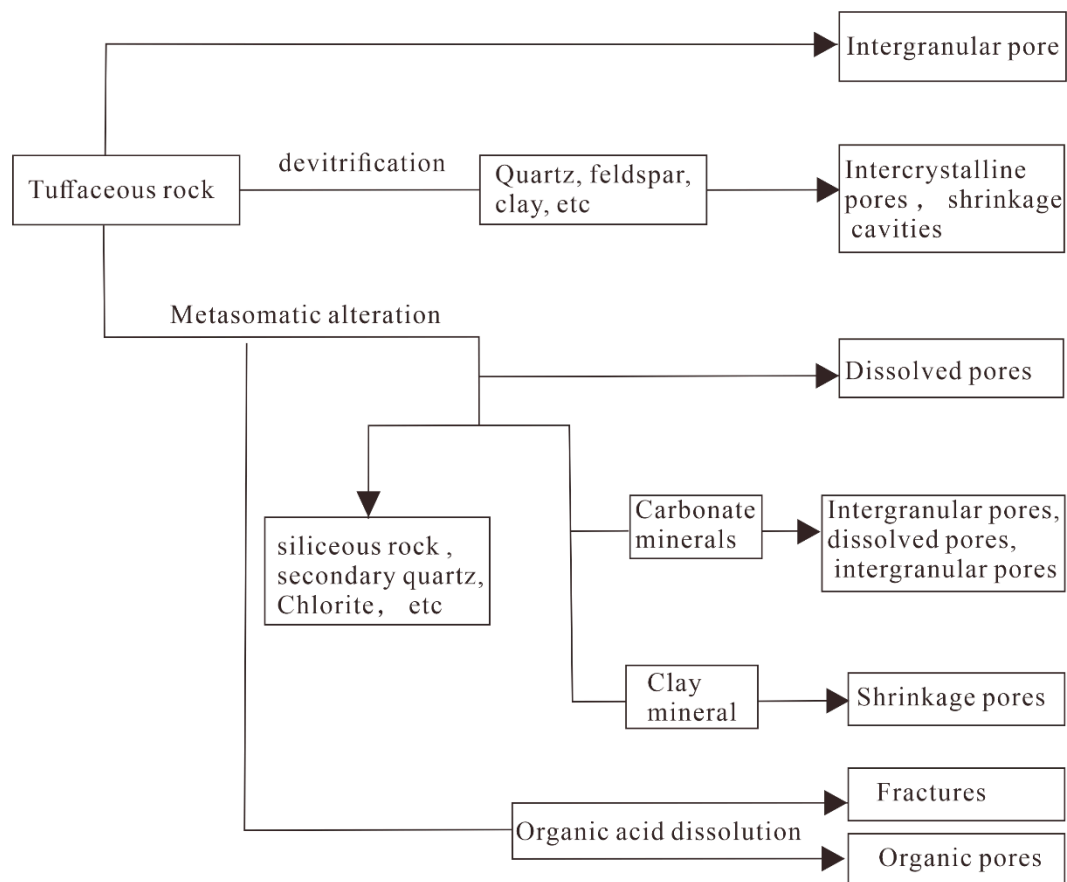


Figure 11. Pore formation and evolution diagram.

6. Conclusions

Focusing on the marine tuffaceous rocks, this study uses field outcrop, thin section, scanning electron microscopy and whole-rock X-ray diffraction experiments to investigate the lithofacies characteristics and the controlling factors of pores, and has gained the following five insights.

- (1) The Permian tuffaceous rocks in the Sichuan Basin are divided into three main lithofacies types, including tuff, sedimentary tuff, and tuffaceous mudstone. The tuffs mainly include detritus tuff and crystal tuff. The sedimentary tuff and tuffaceous mudstone often occur interbedded and are stratified. The mineral composition of the three lithofacies includes quartz, feldspar, carbonate minerals, pyrite, and clay, and the feldspar is mainly potassium feldspar. The tuffs have the highest feldspar, quartz and pyrite content, and the lowest clay and TOC content. The tuffaceous mudstones have the highest clay and TOC content and the lowest feldspar and quartz and pyrite content. The sedimentary tuffs are intermediate between the tuff and tuffaceous mudstone.
- (2) The pore types in the tuffaceous rocks mainly include shrinkage pores, dissolved pores, intergranular pores, organic pores. Shrinkage pores mainly include shrinkage pores formed during the alteration of pyroclastic material and inter-clay shrinkage pores. Shrinkage pores are the common type, usually at the nano-scale, accounting for 81.9% of the total pores. Organic pores account for 11.2% of the total pore space.
- (3) The feldspar and quartz content, and pyrite content in the tuffaceous rocks are inversely correlated with porosity, while the clay content and TOC content are positively correlated with porosity. The higher the tuff content in the three lithofacies, the lower the porosity; therefore, tuff has the lowest porosity, followed by sedimentary tuff, and tuffaceous mudstone has the highest porosity.

- (4) Tuffaceous rocks form many micropores in the process of devitrification. Organic matter pyrolysis and organic acid dissolution also increase the reservoir space and porosity for the reservoir.
- (5) The marine tuffaceous rocks have an overall high TOC content and porosity, and thus have a hydrocarbon generation capacity and reservoir space. They could be hydrocarbon source rocks and reservoirs. As a new type of reservoir, they could form self-accumulation and self-reservoir types of tight reservoirs, with the characteristics of co-generation of the source and reservoir, lithology reservoir, and broad plane distribution, and thus they have great exploration prospects.

Author Contributions: Conceptualization, R.L., Z.W.; methodology, J.H.; result analysis, R.L., Z.W.; experiments, Z.X., W.X.; field observation and sample collection, W.L.; writing—original draft preparation, R.L.; writing—review and editing, Z.W.; supervision, Z.W.; project administration, Z.X.; funding acquisition, W.X. All authors have read and agreed to the published version of the manuscript.

Funding: This research was supported by the Major Scientific and Technological Project of PetroChina (Grant Nos. 2021DJ0605).

Institutional Review Board Statement: Not applicable.

Informed Consent Statement: Not applicable.

Data Availability Statement: The data presented in this study are available on request from the corresponding author.

Conflicts of Interest: The authors declare no conflict of interest.

References

1. Vernik, L. A new type of reservoir rock in volcanoclastic sequences. *AAPG Bull.* **1990**, *74*, 830–836. [[CrossRef](#)]
2. Cao, Y.C.; Jiang, Z.X.; Qiu, L.W. Study on the type and origin of the reservoir space of igneous oil reservoir in Shang 741 Block, Huimin Depression, Shandong. *Acta Petrol. Sin.* **1999**, *15*, 129–136, (In Chinese with English Abstract).
3. Levin, L.E. Volcanogenic and volcanoclastic reservoir rocks in Mesozoic-Cenozoic island arcs: Examples from the Caucasus and the NW Pacific. *J. Pet. Geol.* **1995**, *18*, 267–288. [[CrossRef](#)]
4. Schutter, S.R. Occurrences of hydrocarbons in and around igneous rocks. *Geol. Soc. Lond. Spec. Publ.* **2003**, *214*, 35–68. [[CrossRef](#)]
5. Gecer, B.A. Diagenesis of tipper Eocene volcanoclastic rocks and its relevance to hydrocarbon exploration in the Thrace Basin, Turkey. *Energy Sources* **2006**, *28 Pt A*, 1039–1049.
6. Ma, X.H.; Xu, C.C.; Li, G.H.; Ying, D.L.; Zhang, B.J.; Li, Y.; Dai, X.; Fan, Y.; Zeng, Y.X. Distribution and gas bearing properties of Permian igneous rocks in Sichuan Basin SW China. *Pet. Explor. Dev.* **2019**, *46*, 216–225. [[CrossRef](#)]
7. Zhang, J.; Liu, G.; Cao, Z.; Tao, S.; Felix, M.; Kong, Y.; Zhang, Y. Characteristics and formation mechanism of multi-source mixed sedimentary rocks a saline lake. an ease study of the Permian Lucaogou Formation in the Jimu-Saer Sag, northwest China. *Mar. Pet. Geol.* **2019**, *102*, 704–724. [[CrossRef](#)]
8. Lenhardt, N.; Götz, A.E. Volcanic settings and their reservoir potential: An outcrop analog study on the Miocene Tepoztlán Formation, Central Mexico. *J. Volcanol. Geotherm. Res.* **2011**, *204*, 66–75. [[CrossRef](#)]
9. Huang, K.; Opdyke, N.D. Magnetostratigraphic investigations on an Emeishan basalt section in western Guizhou Province, China. *Earth Planet. Sci. Lett.* **1998**, *163*, 1–14. [[CrossRef](#)]
10. Zhou, M.F.; Malpas, J.; Song, X.Y.; Robinson, P.T.; Sun, M.; Kennedy, A. A temporal link between the Emeishan large igneous province (SW China) and the end-Guadalupian mass extinction. *Earth Planet. Sci. Lett.* **2001**, *196*, 113–122. [[CrossRef](#)]
11. Ali, J.R.; Thompson, G.M.; Song, X.Y.; Wang, Y.L. Emeishan Basalts (SW China) and the ‘end-Guadalupian’ crisis: Magnetobiostratigraphic constraints. *J. Geol. Soc.* **2002**, *159*, 21–29. [[CrossRef](#)]
12. Zhang, H.F.; Wu, X.S.; Wang, B.; Duan, Y.J.; Qu, Y.; Chen, D.F. Research Progress of the Enrichment Mechanism of Sedimentary Organics in Lacustrine Basin. *Acta Sedimentol. Sin.* **2006**, *34*, 463–477, (In Chinese with English Abstract). [[CrossRef](#)]
13. Zhong, H.; Zhu, W.G.; Chu, Z.Y.; He, D.F. SHRIMP U-Pb zircon geochronology, geochemistry, and Nd-Sr isotopic study of contrasting granites in the Emeishan large igneous province, SW China. *Chem. Geol.* **2007**, *236*, 112–137. [[CrossRef](#)]
14. Peate, I.U.; Bryan, S.E. Re-evaluating plume-induced uplift in the Emeishan large igneous province. *Nat. Geosci.* **2008**, *1*, 625–629. [[CrossRef](#)]
15. Hong, Z.; Zhu, W.G.; Hu, R.Z.; Xie, L.W.; He, D.F.; Feng, L.; Chu, Z.Y. Zircon U-Pb age and Sr-Nd-Hf isotope geochemistry of the Panzhihua A-type syenitic intrusion in the Emeishan large igneous province, southwest China and implications for growth of juvenile crust. *Lithos* **2009**, *110*, 109–128. [[CrossRef](#)]
16. Wignall, P.B.; Sun, Y.; Bond, D.P.G.; Izon, G.; Newton, R.J. Volcanism, Mass Extinction, and Carbon Isotope Fluctuations in the Middle Permian of China. *Science* **2009**, *342*, 1179–1182. [[CrossRef](#)]

17. Shellnutt, J.G.; Denyszyn, S.W.; Mundil, R. Precise age determination of mafic and felsic intrusive rocks from the Permian Emeishan large igneous province (SW China). *Gondwana Res.* **2012**, *22*, 118–126. [[CrossRef](#)]
18. Zhu, J.; Zhang, Z.C. The Link between Large igneous provinces and the two mass extinction events in Permian: Review of recent progress the Permian. *Geol. Rev.* **2013**, *1*, 137–148, (In Chinese with English Abstract).
19. Tian, J.; Lin, X.; Guo, W.; Zhang, X.; Huang, P. Geological significance of oil and gas in the eruption event in Sichuan Basin Permian basalt China. *J. Cheng Du Univ. Technol. Sci. Technol. Ed.* **2017**, *44*, 14–20. (In Chinese with English Abstract) [[CrossRef](#)]
20. Ma, X.H.; Yang, Y.; Zhang, J.; Xie, J.R. A Major discovery in Permian volcanic rock gas reservoir exploration in the Sichuan Basin and its implications. *Oil Gas Geol.* **2019**, *39*, 1–8. [[CrossRef](#)]
21. Wen, L.; Li, Y.; Yi, H.Y.; Liu, X.; Zhang, B.J.; Qiu, Y.C.; Zhou, G.; Zhang, X.H. Lithofacies and reservoir characteristics of Permian volcanic rocks in the Sichuan Basin. *Oil Gas Geol.* **2019**, *39*, 17–27. [[CrossRef](#)]
22. Liu, K.L.; Yang, S.; Chen, H.D.; Li, Q.; Ma, L.; Zhang, C.G. Characteristics and evolution of Permian volcanic rocks in Huayingshan area, eastern Sichuan basin. *Miner. Petrol.* **2020**, *40*, 37–49. (In Chinese with English Abstract)
23. Hu, D.F. Breakthrough in natural gas exploration in the platform margin shoal at the Maokou Fm in the Yuanba area, Sichuan Basin, and its implications. *Oil Gas Geol.* **2019**, *39*, 1–10. (In Chinese with English Abstract) [[CrossRef](#)]
24. Tian, X.W.; Luo, B.; Sun, Y.T.; Liu, R.; Li, Y.; Chen, Y.Q.; Zhou, C.L.; Wang, H.; Li, Y.D.; Wang, W.; et al. Natural Gas Characteristics and Source Analysis of Permian Volcanic Gas Reservoir: A Case Study of Well Y1 in Chengdu-Jianyang Area, Sichuan Basin. *J. Jilin Univ. Earth Sci. Ed.* **2021**, *51*, 325–335. (In Chinese with English Abstract)
25. Streck, M.J.; Gruner, A.L. Crystallization and welding variations in a widespread ignimbrite sheet: The Rattlesnake Tuff, eastern Oregon, USA. *Bull. Volcanol.* **1995**, *60*, 545–567. [[CrossRef](#)]
26. Wilson, C.J.N.; Hildreth, W. Assembling an ignimbrite: Mechanical and thermal building blocks in the Bishop Tuff, California. *J. Geol.* **2003**, *111*, 653–670. [[CrossRef](#)]
27. Inoue, A.; Meunier, A.; Beaufort, D. Illite-smectite mixed-layer minerals in felsic volcanoclastic rocks from well drilling cores, Kakkonda, Japan. *Clay Min.* **2004**, *52*, 66–84. [[CrossRef](#)]
28. Ddani, M.; Meunier, A.; Zahraoui, M.; Beaufort, D.; El Wartiti, M.; Fontaine, C.; Boukili, B.; El Mahi, B. Clay mineralogy and chemical composition of bentonites from the Gourougou volcanic massif (northeast Morocco). *Clay Min.* **2005**, *53*, 250–267. [[CrossRef](#)]
29. Garcia-Romero, E.; Vegas, J.; Baldonado, J.L.; Marfil, R. Clay minerals as alteration products in basaltic volcanoclastic deposits of La Palma (Canary Islands, Spain). *Sediment. Geol.* **2005**, *174*, 237–253. [[CrossRef](#)]
30. Cheng, R.H.; Shen, Y.J.; Yan, J.B.; Li, Q.F.; Li, X.H.; Wang, Y.W.; Li, F.; Xu, Z.J. Diagenesis of volcanoclastic rocks in Hailaer basin. *Acta Petrol. Sinica* **2010**, *26*, 47–54, (In Chinese with English Abstract).
31. Yanik, G.; Esenli, F.; Uz, V.; Esenli, V.; Uz, B.; Kuelah, T. Ceramic properties of kaolinized tuffaceous rocks in Kesan region, Thrace, NW Turkey. *Appl. Clay Sci.* **2010**, *48*, 499–505. [[CrossRef](#)]
32. Wang, W.W.; Jang, Z.X.; Xie, X.Y.; Guo, J.X.; Yang, Y.P. Sedimentary characteristics and interactions among volcanic, terrigenous and marine processes in the Late Permian Kuishan Member, Eastern Block of the North China Craton. *Sediment. Geol.* **2020**, *407*, 105741. [[CrossRef](#)]
33. Xiang, F.; Yu, X.; Huang, H.; Zhang, D.; Zhu, X. Mineralogical characterization and diagenetic history of Permian marine tuffaceous deposits in Guangyuan area, northern Sichuan basin, China. *Mar. Pet. Geol.* **2021**, *123*, 104744. [[CrossRef](#)]
34. Fan, X.Y.; He, L.; Zhang, Q.G.; Zhao, P.F.; Zhang, M.M.; Yao, B.W.; Ran, J.W.; Song, J.C.; Li, K.R. Effect of hydration on Pore Structure and Physical Properties of Permian Basalt and tuff in Sichuan Basin during pressurized imbibition. *J. Pet. Sci. Eng.* **2022**, *213*, 10332. [[CrossRef](#)]
35. Li, Q.; Lu, H.; Li, J.; Wu, S.; Wu, Y.; Wen, L.; He, Y.; Qi, F. Characteristics and Formation Mechanism of the Tight Tuff Reservoirs of the Upper Triassic Chang 7 Member in the Southern Ordos Basin, China. *Mar. Pet. Geol.* **2022**, *139*, 105625. [[CrossRef](#)]
36. Tian, Y.; Zhang, X.Y.; He, Y.B.; Luo, J.X.; Zhou, H.; Zhou, X.P.; Du, H.Q. Lithofacies paleogeography of Late Permian Wujiaping in Sichuan Basin. *J. Paleogeography* **2010**, *12*, 164–176. (In Chinese with English Abstract)
37. He, J.; Zheng, R.C.; Hu, X.; Zhang, B.J.; Yin, H.; Ma, H.L.; Wang, Y.; Feng, C.Q. Sedimentary system of the Late Permian Wujiaping Formation in the western Sichuan Basin. *Oil Gas Geol.* **2015**, *36*, 87–95. (In Chinese with English Abstract) [[CrossRef](#)]
38. Tian, Y. Lithofacies Palaeogeography of the Upper Permian Wujiaping Period in the Sichuan Basin. Master's Thesis, China University of Geosciences, Beijing, China, 2018.
39. Xia, M.L.; Wen, L.; Li, Y.; Luo, B.; He, K.L.; Liu, R.; Qiu, Y.C.; He, Q.L.; Chen, K. Permian volcanic eruption cycle, environment and model in the Jianyang area of the Sichuan Basin. *Oil Gas Geol.* **2020**, *40*, 11–22, (In Chinese with English Abstract).
40. Zeng, Q.; Tian, Y.Y.; Zheng, C.; Wang, X.L.; Li, R.R. Distribution of sedimentary tuff in Wujiaping Formation, northwestern Sichuan Basin and Its geological significance. *Nat. Gas Technol. Econ.* **2020**, *14*, 20–26, (In Chinese with English Abstract). [[CrossRef](#)]
41. Peng, H.; Yin, C.; He, Q.L.; Xia, G.Y.; Liu, Y.; Ma, T.H.; Chen, K.; Liu, R.; Su, W. Development characteristics and petroleum geological significance of Permian pyroclastic flow volcanic rocks in Western Sichuan Basin, SW China. *Pet. Explor. Dev.* **2022**, *49*, 56–67, (In Chinese with English Abstract). [[CrossRef](#)]
42. Schmid, R. Descriptive nomenclature and classification of pyroclastic deposits and fragments. *Geol. Rundschau* **1981**, *70*, 794–799. [[CrossRef](#)]

43. Rossignol, C.; Hallot, E.; Bourquin, S.; Poujol, M.; Jolivet, M.; Pellenard, P.; Ducassou, C.; Nalpas, T.; Heilbronn, G.; Yu, J.; et al. Using volcanoclastic rocks to constrain sedimentation ages: To what extent are volcanism and sedimentation synchronous? *Sediment. Geol.* **2019**, *381*, 46–64. [[CrossRef](#)]
44. Schmincke, H.U. *Volcanism*; Springer: Berlin/Heidelberg, Germany, 2004. [[CrossRef](#)]
45. Jones, M.T.; Gislason, S.R. Rapid releases of metal salts and nutrients following the deposition of volcanic ash into aqueous environments. *Geochim. Et Cosmochim. Acta* **2008**, *72*, 3661–3680. [[CrossRef](#)]
46. Song, G.X.; Qin, K.Z.; Li, G.M.; Wang, L. Basic characteristics and research progresses of intermediate sulfidation type epithermal gold poly-metallic deposits, and prospects. *Acta Petrol. Sin.* **2018**, *34*, 748–762, (In Chinese with English Abstract).
47. Jiang, Z.F. Influence of Volcanic Ash on Source Rock Organic Matter Enrichment in the Lucaogou Formation, the Jimusar Depression. Master's Thesis, China University of Petroleum (East China), Dongying, China, 2019. (In Chinese with English Abstract).
48. Li, J.Q.; Lu, S.F.; Cai, J.C.; Zhang, P.F.; Xue, H.T.; Zhao, X.B. Adsorbed and free oil in lacustrine nanoporous shale: A theoretical model and a case study. *Energy Fuels* **2018**, *32*, 12247–12258. [[CrossRef](#)]
49. Li, J.Q.; Lu, S.F.; Xie, L.J.; Zhang, J.; Xue, H.T.; Zhang, P.F.; Tian, S.S. Modeling of hydrocarbon adsorption on continental oil shale: A case study on n-alkane. *Fuel* **2017**, *206*, 603–613. [[CrossRef](#)]
50. Zou, C.N.; Zhu, R.K.; Bai, B.; Yang, Z.; Wu, S.T.; Su, L.; Dong, D.Z.; Li, X.J. First discovery of nano pore throat in oil and gas reservoir in China and its scientific value. *Acta Petrol. Sin.* **2011**, *27*, 1857–1864, (In Chinese with English Abstract).

Disclaimer/Publisher's Note: The statements, opinions and data contained in all publications are solely those of the individual author(s) and contributor(s) and not of MDPI and/or the editor(s). MDPI and/or the editor(s) disclaim responsibility for any injury to people or property resulting from any ideas, methods, instructions or products referred to in the content.